Open Journal of Geology, 2022, 12, 250-272
https://www.scirp.org/journal/ojg
ISSN Online: 2161-7589
ISSN Print: 2161-7570

Geochemistry of Magmatic Rocks of the Syama Belt, Southern Mali, West African Craton

Dasso Yollande Traoré[1*], Seko Sanogo[2], Adama Youssouf Koné[1*], Ismaïla N'Diaye[1], Mamadou Lamine Bouaré[3], Didier Béziat[4]

[1]Laboratoire de Cartographie, DER de Géologie, Faculté des Sciences et Techniques (FST), Université des Sciences, des Techniques et des Technologies de Bamako (USTTB), Bamako, Mali
[2]Laboratoire de Minéralogie et de Pétrologie, DER de Géologie, Faculté des Sciences et Techniques, Université des Sciences, des Techniques et des Technologies de Bamako, Bamako, Mali
[3]Ecole Nationale d'Ingénieurs Abdramane Baba Touré (ENI-ABT), Bamako, Mali
[4]Université Paul Sabatier de Toulouse, Toulouse, France
Email: *dassoyolande@yahoo.fr, *koneadama2005@gmail.com, ismaila.emk@gmail.com, sekosanogo@fst-usttb-edu.ml, bouamala@yahoo.fr, didier.beziat@get.omp.eu

How to cite this paper: Traoré, D.Y., Sanogo, S., Koné, A.Y., N'Diaye, I., Bouaré, M.L. and Béziat, D. (2022) Geochemistry of Magmatic Rocks of the Syama Belt, Southern Mali, West African Craton. *Open Journal of Geology*, **12**, 250-272.
https://doi.org/10.4236/ojg.2022.123014

Received: January 4, 2022
Accepted: March 19, 2022
Published: March 22, 2022

Copyright © 2022 by author(s) and Scientific Research Publishing Inc.
This work is licensed under the Creative Commons Attribution International License (CC BY 4.0).
http://creativecommons.org/licenses/by/4.0/
Open Access

Abstract

Within southern Mali, the Syama belt constitutes a linear major structure-oriented N-S, which host several gold deposits (e.g., Syama and Tabakoroni) and prospect areas (e.g. Tellem). The Syama Belt is formed by magmatic rocks (basalts, lamprophyres, andesites, dacites and microgranites); sedimentary rocks (shales) and volcano-sedimentary rocks (pyroclastics). The magmatic rocks are divided into two main volcanic series: tholeiitic affinity rocks (basalts and lamprophyres) and calc-alkaline affinity (andesites) that are the most evolved. The field relationships between rocks of these two series suggest that the calc-alkaline series are younger the tholeiitic series. These tholeiitic series present the Mid-Ocean Ridge Basalt (MORB) affinity whereas the calc-alkaline series would be linked to an island arc-type. This coexistence is not an isolated case within the West African Craton (WAC). Otherwise, the Syama belt has all the characteristics of other belts, within which a number of gold deposits are developed, in the WAC.

Keywords

Syama Belt, Magmatic Rocks, MORB, Boualé-Mossi Domain, Southern Mali, West African Craton (WAC)

1. Introduction

The West African Craton (WAC) is the part of Africa which is stabilized around

1700 Ma [1] and is constituted by magmatic, metamorphic and sedimentary rocks (**Figure 1**). These geological formations were shaped during eburnean orogeny [2] [3] [4]. It is established within the WAC, the basic magmatic rocks belong to two series succeeding each other in time: tholeiitic and calc-alkaline, the latter presenting in addition to the basalts a differentiated series up to the dacites and rhyolites [2] [3]. However, the geodynamic context of the genesis of the tholeiitic basaltic rocks is always a subject of discussion. According to previous studies, the tholeiitic magmatism from the Birimian basement would be related to: an oceanic MORB-type [5], an oceanic shelf domain [2] [3] [6] [7] [8] and an island arc domain [9]-[17].

On the other hand, all of the authors admit a subduction context for calc-alkaline rocks [17] [18] [19] [20]. Concerning the magmatic rocks of the Syama belt, the geochemical studies to date focused only on major elements [18] [21]. Analyzed samples were taken from drill cores in order to be as free as possible from supergene alteration due to the tropical climate, a widespread alteration in the study area. The present study was initiated to complete the major elements data by adding traces and rare earth elements (REE) with the aim to: i) accurately identify the mafic rocks (basalts and lamprophyres) as well as the various felsic rock types encountered in the three deposits; ii) propose a geodynamic of these rocks.

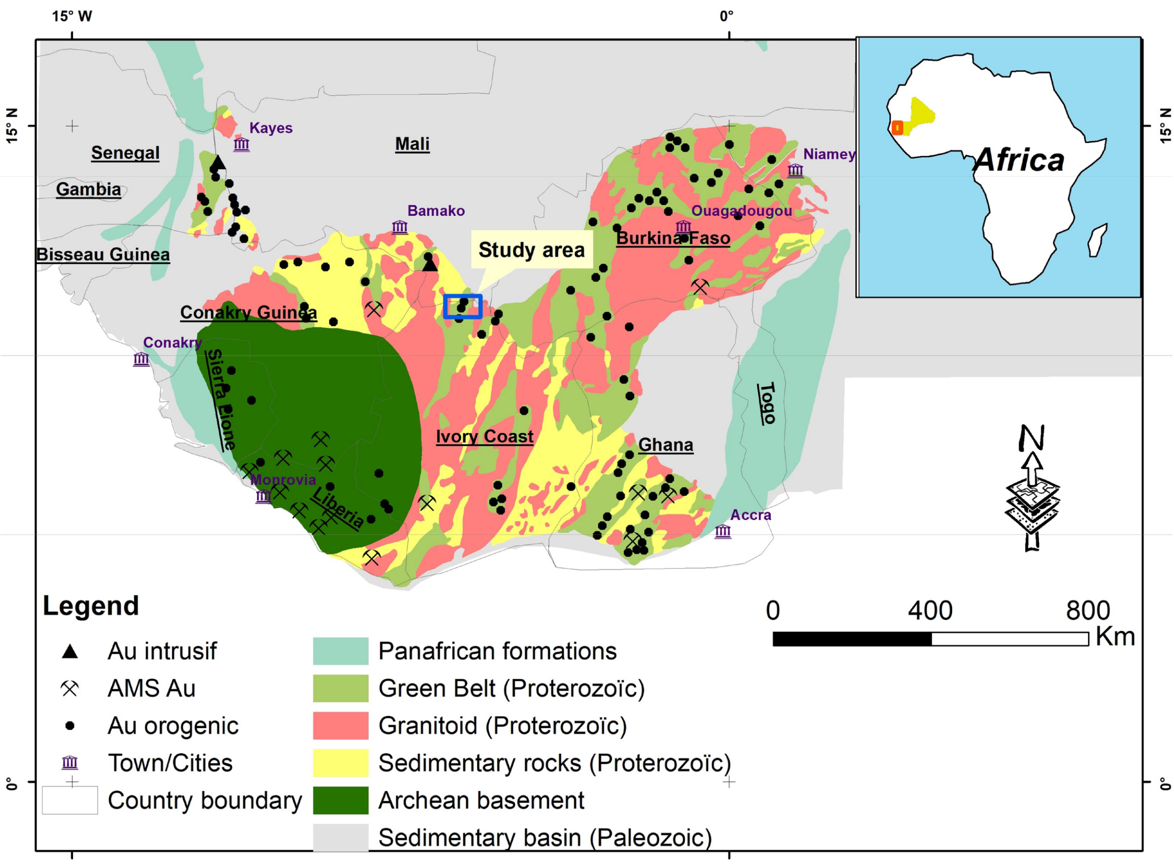

Figure 1. Geological map of Leo-Man Shield with gold showing distribution after [24].

Geological setting

In the WAC, two Precambrian Shields (Reguibat and Leo) and two Precambrian Inliers are noted [1] [22] [23]. This craton is composed of Precambrian formations [1] [24] which are modelled by Eburnean orogeny date to 2.1 Ga [4]. The Leo Shield contains our study area (**Figure 1**) and is situated in the south of Paleozoic basin of Taoudenit.

The eastern part of this shield is composed of Proterozoic formations, also is called the Boualé-Mossi domain. This domain is made up of plutonic, volcano-sedimentary and metamorphic formations that outcrop in Mali in the southern part.

The south of Mali contains five deposits (e.g., Morila, Komana, Kalana, Syama, Tabakoroni) and many gold showing such as Bananso, Syama-extension and Tellem [19] [25] [26] [27] distributed along main shear-zones (e.g., Yanfolila, Banifing, Syama). Along with the Syama shear, three gold deposits (Syama, Tabakoroni and Tellem) are located follow a direction globally N-S (**Figure 2**). This region is formed by a succession of greenstone belts oriented NNE-SSW and separated by sedimentary basins (**Figure 1**). These belts are composed of basic volcanic or sedimentary-dominated volcano-sedimentary rocks and are cross-cut by plutons and granitoid stocks [28]. Among these belts, one of Syama is presented as a narrow belt that extends 100 km within the Banifing shear zone. On the south, it connects to the Sassandra fault in Ivory Coast [29] [30] [31].

The Syama gold deposit as well as ones of Tabakoroni and Tellem is located on the Syama belt (**Figure 2**). These gold deposits are exploited for a long time and are majorly constituted of quartz veins hosted in volcano-sedimentary rocks.

2. Materials and Methods

The main characteristic of the study area is the absence of exploitable outcrops. Indeed, the bedrock is recovered on the surface by several meters thickness of ferruginous lateritic. Therefore, the analyzed samples have been mainly taken from drill cores in order to avoid supergene alteration, which is caused by the tropical climate in the region. Some other samples have been taken from the open pit of Syama. Whole rock geochemical analyses have been performed on 20 representative magmatic rock samples. The choice of these samples was made taking into account the freshness of the rock. The samples have been carefully cleaned and cleared of all surface elements and quartz veins. After, they have been pulverized to avoid any contamination through a long preparation process. Geochemical analysis was performed at Chemex Laboratories in Canada and ALS in Spain.

The ICP-AES (Inductively Coupled Plasma-Atomic Emission Spectrometry) method with lithium tetraborate fusion technique for digestion has been used for samples analysis. This technique was used for geochemistry analysis, in particular the major elements. A prepared sample of 0.200 g is added to the lithium

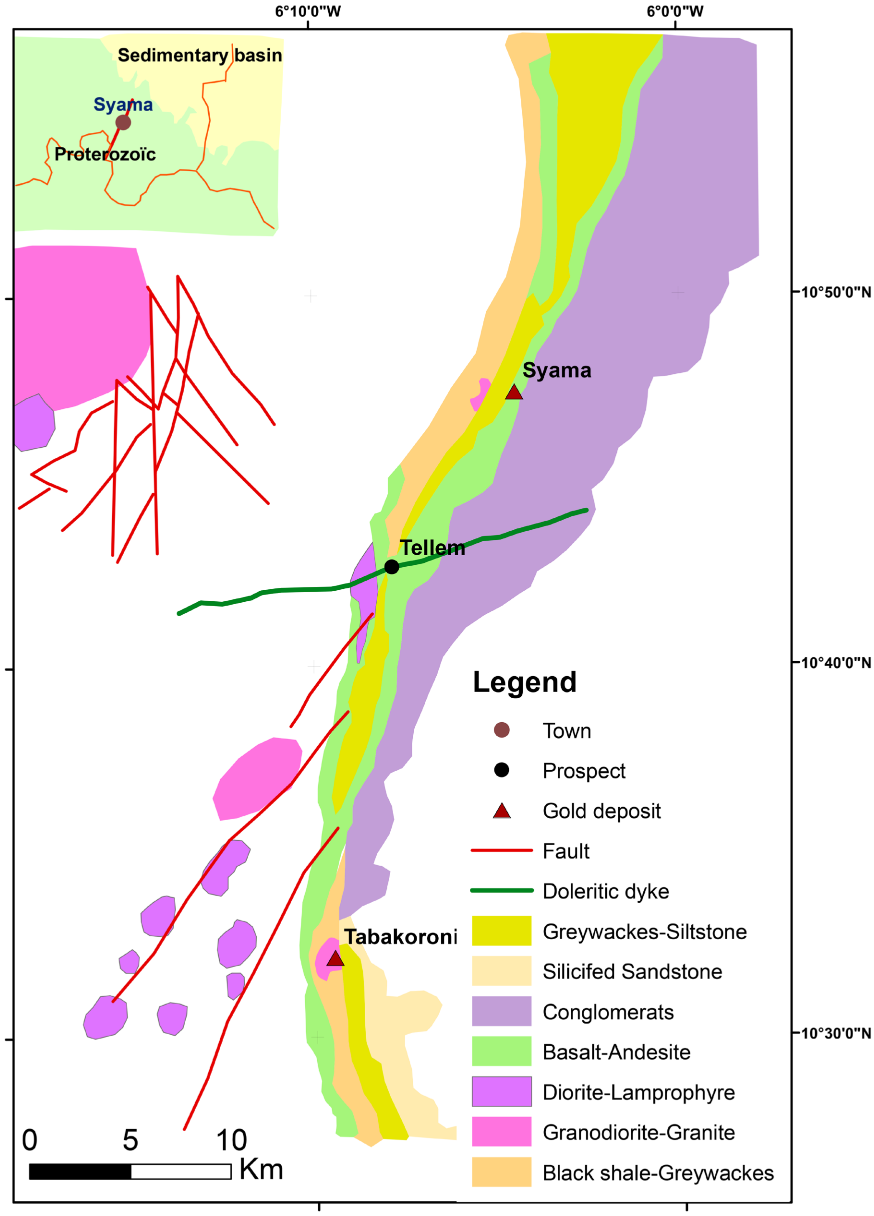

Figure 2. Local geology of the Syama deposit with location of associated deposits and showings, modified from [32].

metaborate/lithium tetraborate of 0.90 g. The whole is mixed well and melted in a furnace at 1000˚C. The resulting melt is then cooled and dissolved in 100 mL of 4% nitric acid or one 2% hydrochloric acid solution. This solution is then analyzed by ICP-AES and the results are corrected in the inter-element spectral interferences. The oxide concentration is calculated from the determined elemental concentration, and the result is reported in a table (**Table 1**).

3. Results

3.1. Classification

The different magmatic rocks of the Syama belt have been defined from the

Table 1. Major and trace elements for 20 representative samples of igneous rocks from the Syama belt. Major elements in % by weight; Trace elements in ppm; <LD = below detection limit.

Litho ID	Basalt								
	Sya Pit2	Sya-MB	Sya 137-5	Sya 243-3	Sya 256-3	Sya 254-3	Tab-2	Tacd 13-1	Tacd-21
SiO_2	48.3	46.7	43	40.7	38.1	49	49.2	47	49.1
TiO_2	1.83	1.1	0.8	0.7	0.69	0.72	1.08	1.16	1.17
Al_2O_3	12.6	10.7	10.85	11.9	10.55	9.34	13.15	12.2	13.15
Fe_2O_3	18.25	12.3	9.02	11.1	9.83	9.32	15.5	16.35	15.7
MnO	0.22	0.14	0.21	0.27	0.22	0.15	0.2	0.22	0.21
MgO	5.43	6.31	6.11	7.77	6.82	9.73	6.06	7.16	6.08
CaO	5.29	6.29	6.7	6.68	10.7	6.91	8.3	9.76	9.02
Na_2O	3.07	2.05	3.22	1.22	1.9	2	2.7	1.92	3.11
K_2O	0.11	0.14	1.61	1.48	1.95	0.03	0.17	0.33	0.13
P_2O_5	0.16	0.09	0.03	0.08	0.04	0.24	0.12	0.11	0.11
BaO	0.01	<LD	0.02	0.02	0.02	<LD	<LD	0.01	0.01
Cr_2O_3	0.01	0.03	0.06	0.02	0.05	0.1	0.05	0.05	0.02
SrO	0.02	0.01	0.03	0.02	0.05	0.02	0.02	0.03	0.02
LOI	5.27	12.55	16.65	16.55	16.8	13.25	2.21	2.14	0.92
Total	100.57	98.41	98.31	98.51	97.72	100.81	98.76	98.44	98.75
As	3.8	64	48	58	42	4	72	69	77
Ba	74.5	27.7	193	223	148.5	28.8	33.5	63.3	63.5
Bi	0.01	9.3	46.4	34.6	114	0.02	3.3	1.8	1.6
C	0.37	2.66	4.5	4.23	4.98	2.78	0.27	0.19	0.05
Co	56	41	31	53	35	47	60	62	57
Cr	70	240	500	140	450	730	410	380	190
Cs	1.96	0.6	1.82	3.66	2.88	0.59	0.65	1.2	0.24
Cu	100	171	104	106	96	60	173	128	140
Ga	19.6	15.4	14	15.2	13.3	14.3	16.8	17.6	16.9
Hf	3.3	2.1	1.6	1.7	1.4	2.8	2.2	2.1	2.3
Hg	0.011	0.03	0.02	0.02	0.2	0.006	0.19	1.2	0.06
Li	30	170	10	80	20	80	30	30	
Mo	1	<LD	10	4	2	<LD	76	<LD	5
Nb	5.1	2.9	2.3	2.2	1.9	4.9	3.1	3.1	3.3
Ni	60	89	166	64	146	270	521	552	122
Pb	<LD	<LD	<LD	2	3	2	<LD	<LD	<LD
Rb	3.6	4.9	48	48.4	52.9	1.1	3.4	11.7	1.7

Continued

S	0.13	0.11	0.06	0.7	1.82	0.13	0.66	0.65	0.08
Sb	1.37	0.01	0.006	0.01	0.048	8.21	0.027	0.015	0.008
Sc	41	41	30	37	28	21	36	40	41
Se	1.3	3.54	31.9	25.2	8.64	0.3	0.71	0.2	0.15
Sr	137.5	90.9	276	147.5	415	204	150.5	227	190
Ta	0.3	0.2	0.1	0.1	0.1	0.3	0.2	0.2	0.2
Te	0.01	0.5	0.4	1	0.9	0.03	1	1.1	0.7
Th	0.55	0.34	0.22	0.55	0.22	2.77	0.32	0.31	0.33
Tl	<LD	0.02	0.02	0.01	0.08		0.07	0.16	0.03
U	1.38	0.36	0.32	0.31	0.27	1.66	0.43	0.44	0.47
V	501	0.11	0.09	0.21	0.07	171	0.11	0.11	0.13
W	1	339	258	242	248	1	388	390	387
Y	38.3	3	31	4	7	16.3	5	3	2
Zn	143	115	60	99	58	87	118	140	116
Zr	115	2.25	2.27	1.98	1.74	106	2.97	3.03	3
La	5.7	3.4	3	4.7	2.4	18.8	4	3.9	4
Ce	15.3	9.1	7.4	11.1	6.4	42.7	10.6	10.6	10.7
Pr	2.44	1.39	1.15	1.45	0.95	5.7	1.63	1.61	1.64
Nd	12.6	6.9	5.1	6.7	4.8	23.2	8.2	8.3	8.1
Sm	4.59	2.23	1.99	1.95	1.75	5.1	2.75	2.78	2.61
Eu	1.46	0.85	0.64	0.76	0.67	1.3	0.99	1.04	1
Gd	5.74	3.12	2.59	2.54	2.45	4.01	3.73	3.86	3.81
Tb	0.99	0.55	0.48	0.47	0.41	0.59	0.65	0.71	0.66
Dy	6.73	3.67	3.27	2.91	2.83	3.38	4.27	4.54	4.24
Ho	1.47	0.74	0.67	0.63	0.59	0.68	0.97	0.97	0.94
Er	4.08	2.39	2.34	1.99	1.85	1.64	3.07	3.15	3.1
Tm	0.64	<LD	<LD	<LD	<LD	0.26	<LD	<LD	<LD
Yb	4.03	22.3	19.8	17.1	16.9	1.43	26.5	27.9	27
Lu	0.62	0.36	0.35	0.29	0.28	0.22	0.46	0.45	0.46

Litho	Lamprophyre				Andesite-dacite		Microgranite				
ID	Tab-204	Sya Pit1	Sya Pit4	Sya B1	Tacd 13-2	Tacd-242	Te 58-1	Te 92-4	Te 92-5	Te 92-6	Te 92-7
SiO_2	42.3	43.3	41.3	37.7	66.8	66.9	71.9	71.8	74.5	71.8	71.1
TiO_2	0.51	0.57	0.6	0.96	0.45	0.41	0.27	0.28	0.27	0.27	0.26
Al_2O_3	10.3	8.93	9.07	13.35	16	15.7	15.05	15.05	14.85	14.45	15.05

Continued

Fe_2O_3	9.98	9.41	6.98	16.85	3.12	3.23	2.02	2.09	2.27	2.22	2.2
MnO	0.17	0.19	0.26	0.16	0.04	0.04	0.01	0.02	0.01	0.04	0.03
MgO	12.85	9.24	7.74	9.79	1.34	1.22	0.7	0.59	0.71	0.64	0.57
CaO	10.05	7.14	12.05	6.6	3.04	2.13	0.21	1.04	0.23	2.48	1.54
Na_2O	0.01	1.12	1.68	1.16	6.01	5.91	4.86	4.75	4.68	4.72	4.6
K_2O	<LD	1.74	1.55	0.11	1.14	1.25	2.25	2.25	2.28	1.87	2.42
P_2O_5	0.19	0.17	0.83	0.25	0.17	0.18	0.11	0.11	0.11	0.1	0.11
BaO	<LD	0.04	0.04	0.01	0.09	0.07	0.08	0.08	0.08	0.09	0.09
Cr_2O_3	0.24	0.16	0.11	0.13	0.03	0.04	<LD	0.01	0.04	0.01	0.03
SrO	0.03	0.03	0.08	0.01	0.13	0.09	0.05	0.07	0.05	0.09	0.06
LOI	12.75	19.7	19.65	14.7	1.63	3.52	1.73	2.39	1.74	3.09	2.73
Total	99.38	101.74	101.94	101.78	99.99	100.69	99.24	100.53	101.82	101.87	100.79
As	77	2	<LD	66.6	110	107	78	74	83	81	79
Ba	3.2	350	371	50.8	832	672	803	694	719	739	775
Bi	56	0.04	0.06	0.04	3.3	102	<LD	<LD	LD	31.5	<LD
C	2.07	5.2	5.1	2.61	0.22	0.65	0.02	0.22	0.02	0.54	0.34
Co	64	44	39	42	12	8	5	5	6	4	5
Cr	1910	1140	740	940	270	280	30	50	290	90	270
Cs	0.37	4.34	2.87	1.12	5	3.62	3.26	3.8	3.36	3.48	3.37
Cu	69	63	43	115	40	35	17	19	19	25	18
Ga	12.9	13	13.8	21.9	22	20.6	20.2	20.9	20.6	19.6	21.3
Hf	2.1	2	3.2	3.6	3.2	3.2	2.8	2.6	2.7	2.8	2.7
Hg	0.16	0.128	0.048	0.006	0.14	0.81	0.16	0.1	0.11	0.16	0.11
Li	50	30	20	270	10	20	20	20	30	10	20
Mo	<LD	1	1	1	34	15	<LD	6	12	8	15
Nb	3	3.9	5.8	5.8	3.2	3.4	4	4.6	4.9	4.6	5.1
Ni	467	340	450	216	200	41	12	34	26	26	36
Pb	3	<LD	5	8	13	7	8	11	12	13	10
Rb	0.3	59.1	48	3.5	37.7	38.9	59.5	64.1	63.2	57.2	66.7
S	0.34	0.04	0.04		0.11	0.34	0.28	0.72	0.56	0.12	0.63
Sb	0.042	14.85	26.4	4.56	0.016	0.071	0.011	0.028	0.038	0.017	0.044
Sc	23	22	15	32	5	4	4	4	4	4	4
Se	0.16	0.2	0.7	0.4	0.57	5.79	1.33	1.02	1.91	0.3	1.36
Sr	224	262	651	106.5	1175	843	476	651	449	789	546
Ta	0.2	0.2	0.3	0.3	0.2	0.2	0.3	0.3	0.3	0.3	0.3

Continued

Te	1.2	0.01	0.02	0.03	0.4	0.5	0.4	0.3	0.5	0.2	0.3
Th	1.51	2.13	7.49	2.51	2.72	2.79	2.76	2.69	2.9	2.64	2.71
Tl	0.04	0.06	0.06	<LD	0.02	0.16	0.02	0.01	0.02	0.01	0.02
U	0.2	2.73	3.67	1.64	0.07	0.07	0.09	0.09	0.09	0.11	0.11
V	0.46	164	125	306	1.35	1.33	1.6	1.65	1.71	1.65	1.73
W	157	13	17	2	54	59	29	30	31	31	31
Y	3	12.2	18.8	21.6	2	19	17	18	25	9	24
Zn	86	71	30	174	67	58	42	52	49	49	57
Zr	1.29	77	145	139	0.5	0.42	0.58	0.58	0.6	0.62	0.6
La	11.2	12.4	79.8	11.7	21.7	23.3	19.2	16.9	16.8	15.6	15.8
Ce	25.7	26.5	176	29.3	44.6	48.3	39.7	34.5	35.5	32.6	33.5
Pr	3.43	3.46	23.4	4.31	5.36	5.73	4.91	4.34	4.37	4.11	4.07
Nd	14.5	14.9	93.2	19.6	20.3	21	18.7	16.4	16.9	15.7	16
Sm	3.37	3.37	16.4	5.05	3.54	3.68	3.52	3.3	3.31	3.2	3.23
Eu	0.77	0.88	3.92	1.25	0.94	1.03	0.89	0.84	0.84	0.99	0.74
Gd	2.85	2.78	9.95	4.37	2.06	2.08	2.36	2.24	2.25	2.13	2.25
Tb	0.43	0.42	1.06	0.67	0.25	0.25	0.29	0.29	0.29	0.3	0.27
Dy	2.45	2.41	4.55	4.19	1.11	1.1	1.43	1.46	1.4	1.5	1.44
Ho	0.5	0.47	0.67	0.84	0.18	0.19	0.22	0.24	0.26	0.28	0.24
Er	1.57	1.38	1.53	2.31	0.57	0.5	0.7	0.63	0.63	0.69	0.68
Tm	<LD	0.21	0.19	0.35	<LD	<LD	<LD	<LD	<LD	<LD	<LD
Yb	13.6	1.27	0.94	2.31	5.6	5.6	7.4	7	7.2	8.3	7.3
Lu	0.2	0.2	0.15	0.36	0.05	0.06	0.08	0.1	0.09	0.1	0.1

classification of [33] (**Figure 3**), sub-alkaline series classification (**Figure 4**) and FeOt/MgO vs SiO_2 distribution (**Figure 5**). The classification is also based on the major elements SiO_2, Na_2O and K_2O and that of Harker trace elements Nb, Y, Zr and Ti (**Figure 6**). These Harker's diagrams are used to assess the degree of fractional crystallization. So, they allow us to understand mineralogical evolution and to highlight the genetic relations between the different magmatic rocks. These classifications complete the results of thin sections of the magmatic rocks with an optical microscope [26].

The two diagrams obtained show that the magmatic rocks in the belt consist of several types: i) a basic set combining basalt and lamprophyre of Syama and Tabakoroni; ii) an intermediate set corresponding to andesitic-dacitic rocks collected at Tabakoroni; iii) a differentiated set corresponding to microgranites at Tellem. In addition, the diagram of [33] shows that the different rocks belong to the sub-alkaline series (**Figure 4**). These rocks have been also plotted in Harker

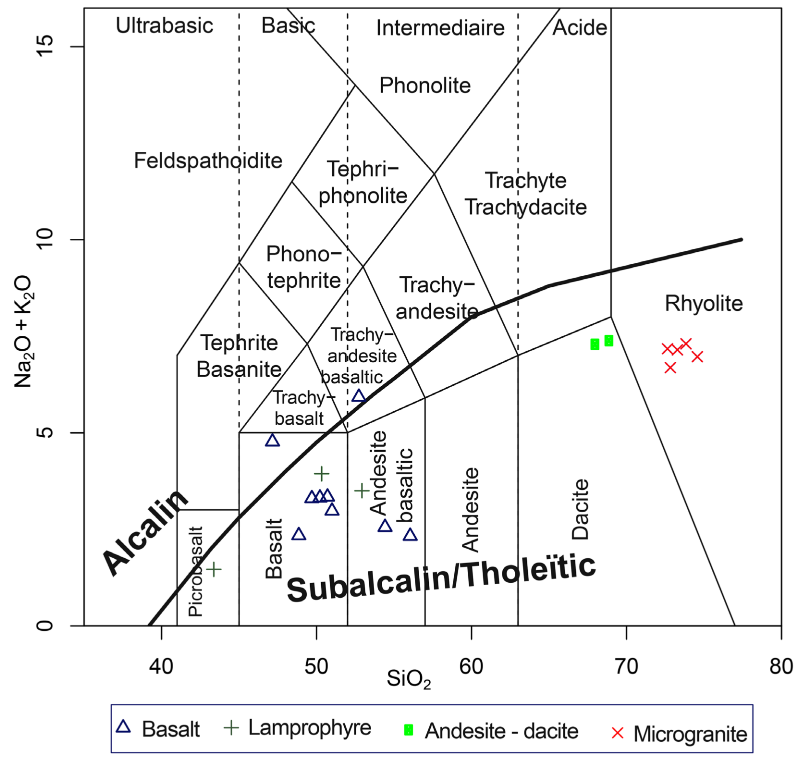

Figure 3. Classification diagram of magmatic rocks of the Syama-Tabakoroni-Tellem zone according to alumina saturation (A/NK as a function of A/CNK) from [34].

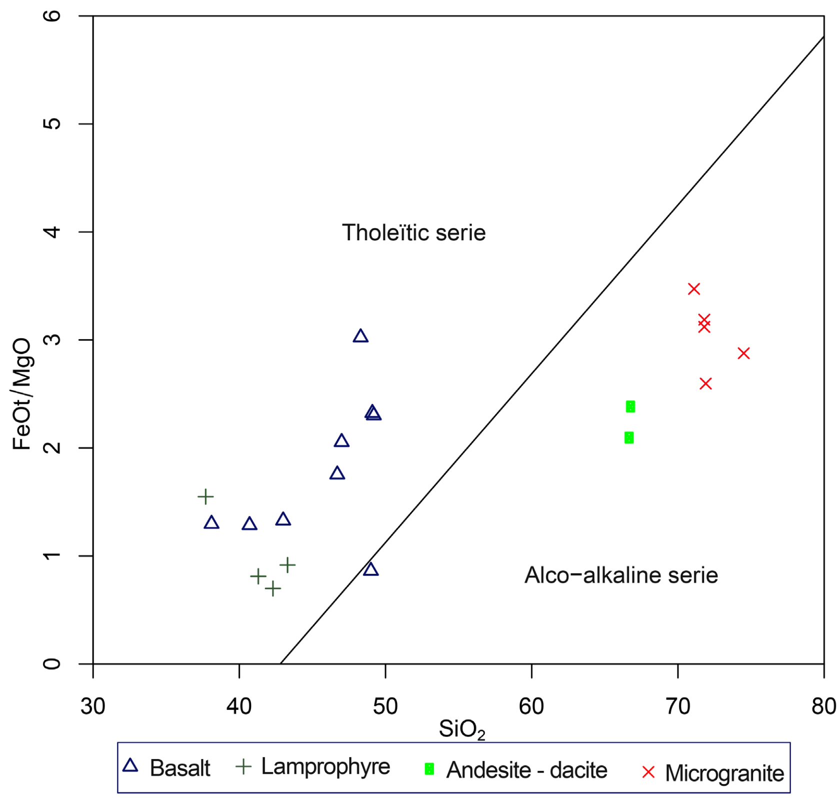

Figure 4. Alkaline-Silica diagram of magmatic rocks of Syama, Tabakoroni and Tellem, modified after [35].

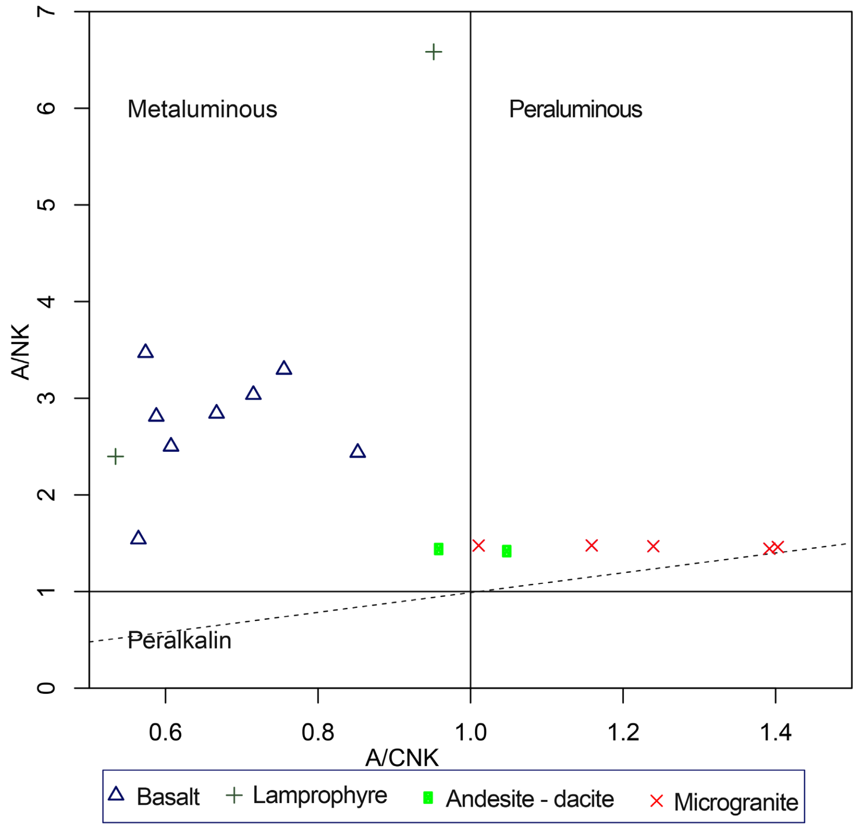

Figure 5. Distribution of magmatic rocks of the Syama-Tabakoroni-Tellem zone according to [39].

diagrams (oxides vs SiO_2) (**Figure 6**), which highlight: i) the dispersion of the data and the absence of correlation between oxides and SiO_2; ii) the variability of the contents of certain oxides such as TiO_2, Na_2O and K_2O within the same petrographic rock type (basalt or lamprophyres) This variability would be related to the differential of hydrothermal alteration.

3.2. Mobility of the Components

Syama belt rocks have undergone strong supergene and hydrothermal alteration. Thus, in order to define the primary characteristics of the magmatic rocks, we chose rocks less affected by silicification phenomena and those where vein networks were less dense.

Major elements analysis shows that supergene alteration is highly variable (**Figures 7(a)-(l)**). It results in a loss on ignition (LOI) of 5% to 17% in the Syama basalts, 1% to 2.2% in the Tabakoroni basalts, 12.7% to 21.8% in the Syama and Tabakoroni lamprophyres, 1.6% to 3.5% in the Tabakoroni andesites, and 1.7% to 3% in the Tellem microgranites. To be sure to characterize the igneous rocks despite the high loss on ignition values and a possible hydrothermal alteration in some facies, we plotted the incompatible element Nb and the trace element Zr (**Figure 7(h)**). The trace element Zr is known to be immobile in even altered mafic volcanic rocks [36] [37] [38]. This diagram shows a good correlation between

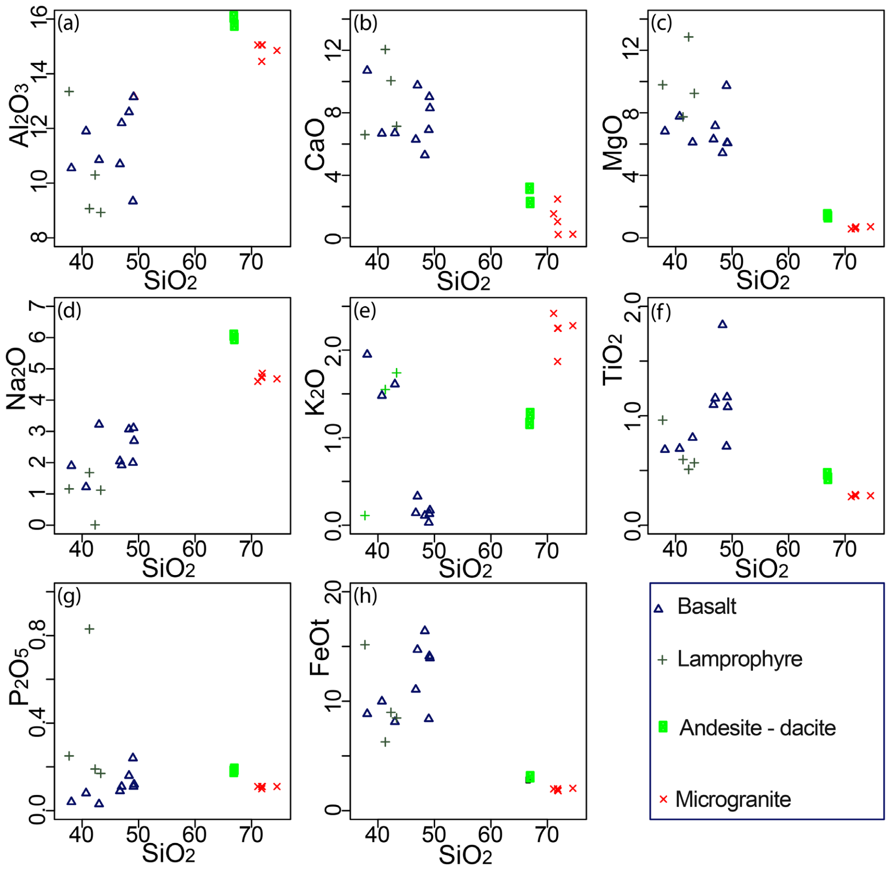

Figure 6. Harker-type variation diagrams of major elements vs SiO_2 of igneous rocks of the Syama-Tabakoroni-Tellem areas showing an absence of discontinuity in the evolution.

the two elements, following a straight line through the origin, indicating that the elements have not been affected by these secondary processes. They can therefore be used to recover the original characteristics of our rocks (Figure 7(h)).

3.3. Rares Earth Elements Spectra

In order to eliminate the variation in abundance between rare earth elements of odd-even atomic numbers, the values of the Syama-Tabakoroni-Tellem magmatic rocks have been normalized with the concentration of the early mantle [40]. This normalization allows us also to discern the extent of any fractionation among rare piles of earth in the studied samples (Figure 8). The rare earth spectra show a general decrease from light rare piles of earth to heavy rare piles of earth except for basalts where the spectra remain constant. These spectra show mostly a positive anomaly in Yb except the spectra of the lamprophyres. The spectra of the different types of rocks are generally cross. However, andesites-dacites and microgranites spectra show parallelism between them.

The spectra most often show a negative anomaly in Eu (Eu/Eu* < 1). This implies that Eu plays an important role in the fractionation of plagioclases by substituting Sr, Ba or Ca (Figure 9). The REE spectrum shows a negative absence of Eu anomaly for all the samples analyzed (Figure 8).

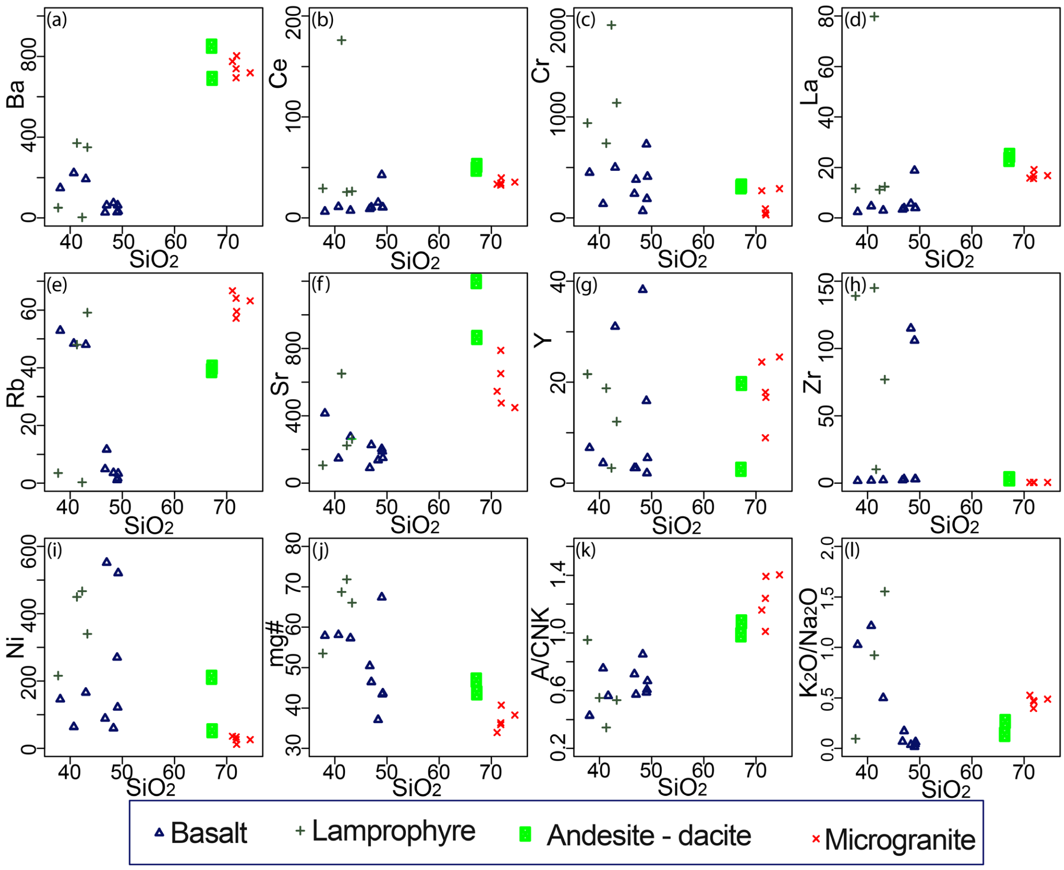

Figure 7. Harker-type variation diagrams of trace elements vs SiO_2 of igneous rocks of the Syama-Tabakoroni-Tellem areas.

The slope (La/Lu) of the spectra is negative, implying that magmatic rocks of Syama-Tabakoroni-Tellem present enrichment in LREE compared to HREE. Except for basalts where the slope is constant, so no enrichment or depletion of LRRE compared to HREE (Figure 8).

3.4. Rares Earth Elements Expanded Spider Diagram

The expanded REE values of the Syama-Tabakoroni-Tellem magmatic rocks have been normalized to the primitive mantle, after [41] to multi-element spider diagrams (expanded REEs). These spider diagrams (Figure 9) show positive anomalies which are characterized by peaks of enrichment. We are noted also negative anomalies marked by indentations of depletion.

As in the REE spectra, these normalized multi-element spider diagrams of the Syama-Tabakoroni-Tellem rocks (Figure 9) are cross, except for the spectra of andesites-dacites and microgranites which are parallel to each other. The lamprophyre spider diagrams are too intersecting and are difficult to interpret, so they are not taken to account in Figure 9.

All the spider diagrams of basalts, andesites-dacites and microgranites show positive anomalies in Cs, K, Sr, Yb and negative anomalies in Rb, Nb, La-Ce, P, Zr, Lu (Figure 9). In addition to these common anomalies, basalts present a

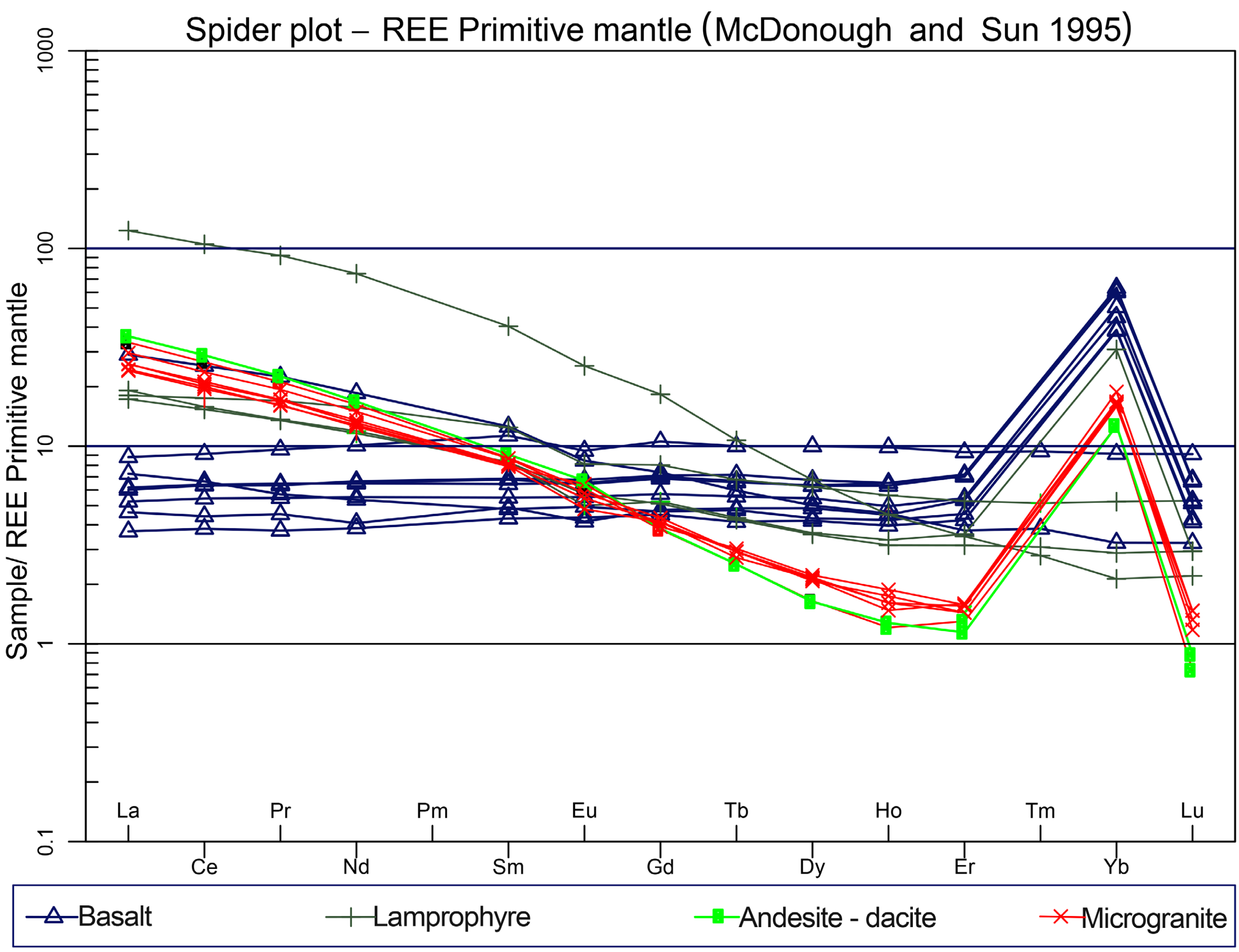

Figure 8. Rare earth spectra of igneous rocks (9 basalts, 4 lamprophyres, 2 andesites-dacites and 5 microgranites) of the Syama-Tabakoroni-Tellem area of the study area normalized to the early mantle [40].

positive anomaly in U and negative anomalies in Ba, Th, Y. On the other hand, andesites-dacites and microgranites present positive anomalies in Ba, Pb, Nd, Sm and negative anomalies in U, Pr, Ti.

3.5. Basalts

Nine Basalt samples have been analyzed whose six at Syama and three at Tabakoroni. Their SiO_2 contents vary from 38 wt% to 49 wt%, ones Fe_2O_3 from 9 to 18 wt% while Al_2O_3, MgO and CaO contents are relatively homogeneous and respectively ~ 12%, ~ 6% with an exception reaching 10%, 6.5% with an exception reaching 10.7%. Cr and Ni contents are high, reaching 730 ppm and 562 ppm respectively in some samples. The basalts are very weakly enriched in REE with a ∑REE varying between 25 and 60 ppm. An exceptional high value is recorded in Syama basalt where the ∑REE reaches 100 ppm related to higher La (19 ppm), Ce (42 ppm) and Nd (25 ppm) contents. In the chondrite-normalized diagram of [41], the basalts show nearly flat rare-earth (REE) spectra (La/Yb CN = 0.95 - 1.70 at Syama, 0.92 - 0.97 at Tabakoroni, devoid of anomaly or with low

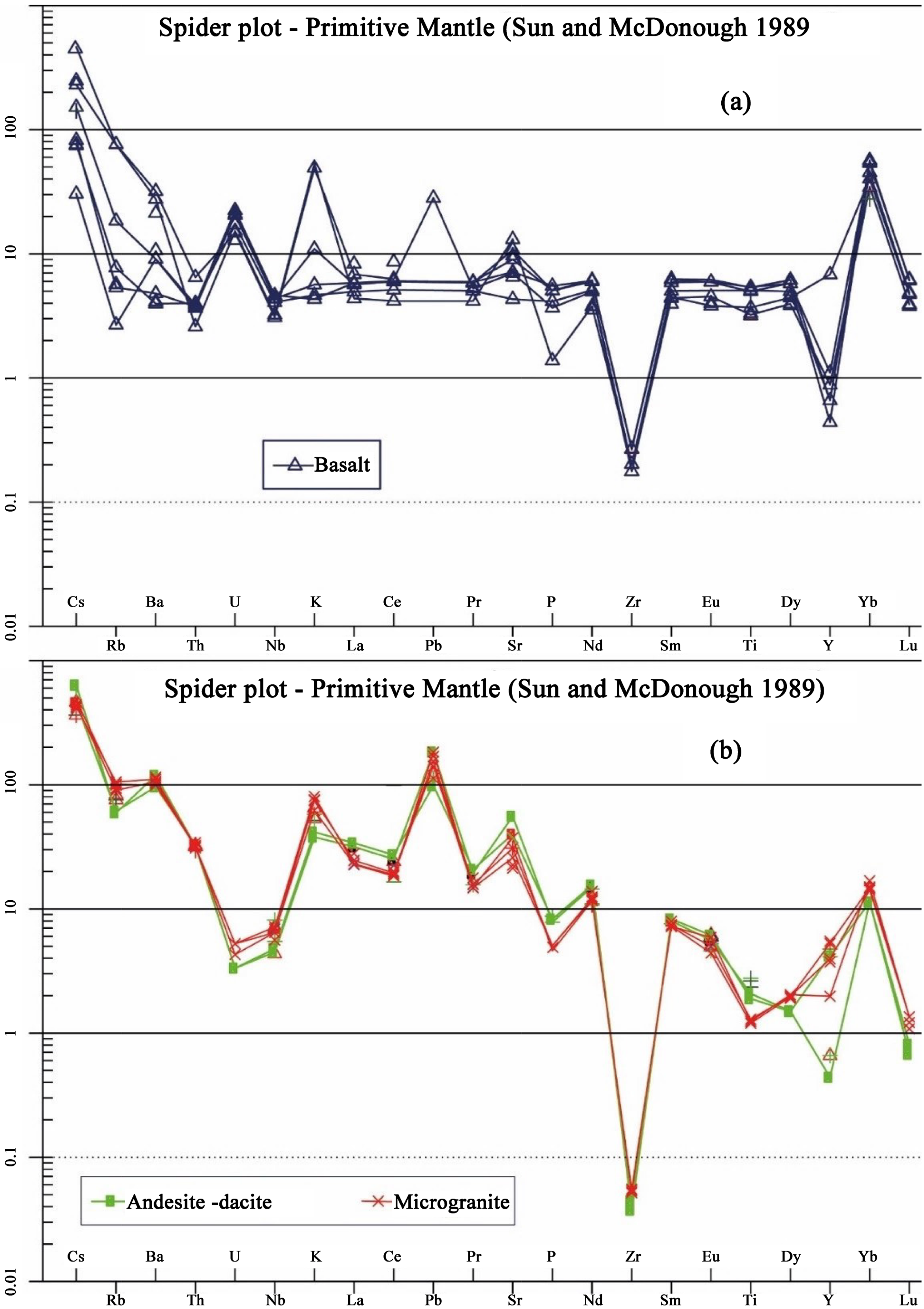

Figure 9. Expanded rare earth spider diagrams of igneous rocks of the Syama-Tabakoroni-Tellem zone normalized to the early mantle [41].

negative europium anomaly (Eu/Eu* = 0.86 - 1.04 at Syama, 0.95 - 0.97 at Tabakoroni). In a multi-element diagram of values normalized to the early mantle data [41], the basalts show some dispersion in alkali element concentrations (Cs, Ba, Rb) related to their mobility but relatively flat spectra, with no negative anomalies in Nb and Ta for the other elements, notably the HFSE (**Figure 9(b)**). These data indicate that crustal contamination did not play an important role in the evolution of the compositions of these magmas [42]. Significant crustal contamination would be indicated by strong negative anomalies in Nb and Ta. Finally, the Zr/Y ratio, lower than 4 (2.6 and 2.8 respectively for Syama and Tabakoroni), would indicate a tholeiitic affinity for these basalts [43]. Indeed this ratio is between 4 and 7 for transitional lavas, and higher than 7 for calc-alkaline lavas.

3.6. Lamprophyre

Five lamprophyre samples collected in Syama and in Tabakoroni have been analyzed. The result shows they present mafic lavas characteristics comparable to basalts (**Figure 5**), and ones of ultramafic rocks. These samples are characterized by a very high value of LOI up to 21 wt%, low contents of SiO_2 ranging from 38 and 43 wt%. The Fe_2O_3 contents are variable (between 7 wt% and 17 wt%) while the ones of MgO are between 7.8 wt% and 10.5 wt%. The major characteristic is their very high content of Cr (up to 1910 ppm) and of Ni (up to 470 ppm). The lamprophyres are enriched in Rare Earth Elements with ∑REE ranging from 47 to 386 ppm. In the chondrite-normalized diagram, the REE shows a good fractionation with (La/Yb) CN between 4 and 61. The Eu anomalies are clearly negative with Eu/Eu* ratio from 0.76 to 0.94. The lamprophyres also show high alkaline concentrations (Cs, Ba, Rb) compatible with their mica richness [27], very high U and Th contents (100 times higher than those in the Primitive Mantle) and evident negative anomalies in Nb and Ta (**Figure 8**). These chemical characteristics are those of calc-alkaline lamprophyres of the spessartite type [44]. They are also similar to calc-alkaline lamprophyres from the Black Mountain [45], eastern Pontides in NE Turkey [46], NW Mexico City [47], and also to lamprophyres from the Daping gold deposit [48].

3.7. Andesite-Dacite

For andesite-dacite, two samples from the Tabakoroni deposit have been analyzed. These samples are characterized by high SiO_2, Al_2O_3, Na_2O contents (respectively equal to 67 wt%, 16 wt% and 6 wt%). They are highly enriched in REE with a ∑REE ranging from 95 to 101 ppm. So, they are highly fractionated with a very high enrichment in light REE (La/YbCN = 31 - 40). In multi-element diagram normalized to the Primitive Mantle (**Figure 8** and **Figure 9(b)**), the andesite-dacite samples show a negative Nb-Ta anomaly. The Zr/Y ratio of the andesites is between 10 and 20, a value compatible with a calc-alkaline affinity. This result is confirmed by the diagram of [49] in which andesitic samples are placed in the calc-alkaline field (**Figure 5**).

3.8. Micrograpnites

The analyzed micrograpnitic vein of Tellem is characterized by high SiO_2 (71 wt% to 74 wt%) and Al_2O_3 (~15 wt%) contents and relatively high K_2O proportion (between 1.87% and 2.42%). It is enriched in REE with ∑REE varying between 47 and 73 ppm and its spectra are strongly fractionated with La/YbCN ranging from 18 to 23 ppm. It generally shows a negative anomaly in Eu (Eu/Eu* = 0.84) with an exceptional positive value (Eu/Eu* = 1.16). However, multi-element diagram shows very strong negative anomalies in Nb, Ta and Th.

4. Discussion

In the Syama belt, three populations of magmatic rocks have been identified: basalts with a tholeiitic affinity, and more advanced rocks (andesites with micrograpnites) and lamprophyres with a calc-alkaline affinity. The intersection between lamprophyric veins and basalts verify the chronology proposed for this birimian period, namely the calc-alkaline event is posterior to the one of tholeiitic.

In order to characterize the tectonic the emplacement context of these various magmas, we consider that the principle of uniformitarianism is verified and that the processes of magma genesis for the Precambrian period are similar to those of the present period [50]. Thus, if we consider current island arc basalts (IABs) we note that the concentrations in Nb (<2 ppm; [51] is lower than basalts from other tectonic settings. This translates into a negative Nb anomaly and also Ta (similar chemical properties to Nb) in diagrams normalized to the early mantle [52]. These chemical characteristics are found in many tholeiitic basalt suites of Precambrian greenstone belts that have then been interpreted as formed in an arc setting [50] [51] [53].

In Syama belt, the basalts do not show negative anomalies of Nb and Ta, but relatively REE flat spectra. This type of spectrum is characteristic of basaltic sequences in current oceanic shelves (e.g. Nauru).Thus, a contextual analogy has been considered for similar ancient oceanic shelf basaltic sequences [2] [54]. To discuss the composition of mantle sources, [37] instead favors elemental ratios using HFSEs, as these elements have similar incompatibilities in the mantle. Thus, the author’s diagram combining Zr/Nb ratios with Nb/Th applied to the Syama and Tabakoroni basalt samples would indicate an oceanic shelf signature for them.

For differentiated rocks (andesite and micrograpnite), data strongly fractionated spectra (**Figure 8**), and the negative anomalies in Nb, Ta, Zr/Nb on Nb/Th ratios (**Figure 9(b)**), indicate the arc magmatism type.

Within the WAC, the tholeiitic basalts, which have the same characteristics as those of the Syama belt [2] [11] have been interpreted differently. Thus, [5] considers the Birimian tholeiitic basalts of the WAC as MORB equivalents. However, many authors [9]-[17] propose an o island arc context for these basalts. Finally, an oceanic shelf tectonic environment in relation to a mantle plume has been considered by [2] for the tholeiitic basalts (2.1 Ga) of the WAC parts (e.g., Mauritania, Senegal, Burkina-Faso), by [6] for volcanics from northeastern Ivory Coast, by [7] for volcanics from the Kédougou-Kéniéba Inlier (eastern Senegal), and recently by [8], for metavolcanics from the neighboring Mana district in the Houndé belt of Burkina Faso. Similarly, [55] proposed for the iron-rich tholeiitic basalts of the Birimian-aged El Callao formation, located on the Guiana Shield (equivalent to the WAC for the South American craton), an oceanic shelf tectonic setting. However, in this last example, in addition to the large volume of basalt (maximum thickness estimated at 1200 m), the existence of komatiite-type formations underlying the basalts has been highlighted, formations that have not been recognized to date in the WAC. In these last two examples (Mana and El Callao), the tholeiitic basaltic formations are host to gold mineralization. The same remark is done in Syama deposit.

The absence of isotopic data, the state of alteration affecting rocks and the poor conditions of outcrop does not make it possible to estimate the real volume of these various formations. It is thus difficult in our case to define precisely the tectonic context of these tholeiitic basalts.

In the Syama region, calc-alkaline formations are represented by mafic plutonic (lamprophyres) and more differentiated rocks (andesites and microgranites). The existence of mafic rocks (ultrabasic to basic) belonging to the calc-alkaline series was shown by [13] in the Loraboué region (Burkina Faso) and by [56] in the Kadiolo belt, located to the east of Syama belt.

The differentiated rocks of the Syama belt show strong similarities with the rocks of the calc-alkaline series of the Kédougou buttonhole in Senegal [57], Guinea [58] or Kalana in the south-east of Syama in Mali [25]. For the emplacement of the calc-alkaline rocks of the WAC belts, an island arc setting has been very often proposed [2] [9]-[17]. For the Bagoé belt, [18] [21] also proposed an origin in a back-arc context, and the Kadiana Madinani domain terrains are interpreted as a back-arc basin. Similarly, [57] proposed an island arc context for the emplacement of a set of ultramafic to mafic rocks of the Kadiolo belt, located east of the Syama belt. In conclusion, the calc-alkaline series represented by the differentiated volcanic rocks would be developed in an island arc context.

As for the spessartite lamprophyres, it is important to note that they are frequently found in association with gold mineralization. This is the case in Archean terrains, such as in Matheson, in Ontario [58] [59] and the Yilgarn Craton, Australia [60], but also in Cenozoic formations such as in China's Yunnan Province with the Daping gold deposit, located along the Ailao-Shan-Red-River gold shear-zone, the latter being related to the collision of the Indian and Eurasian plates [48]. These various authors consider that this type of magmatic rock would be set up late during the geodynamic evolution, during late transmission to post-collisional tectonic phase. These particular rocks, rich in compatible (Cr and Ni) and incompatible (LILE and HFSE) elements would derive from magmas generated from a metasomatized mantle source [44] [46]. So, this origin is generally the case for this type of highly potassic-rich magma. In the case of Syama, the lamprophyres, intersecting the basalts in the belt, would mark the first extensive post-collisional stages that would take place at the end of the Eburnian orogeny.

5. Conclusions

The coexistence of heterogeneous geochemical signatures of igneous rocks in the Syama Belt (tholeiitic and then calc-alkaline), suggests that the rocks were formed in different tectonic settings during the Eburnian orogeny.

The coexistence of tholeiitic and calc-alkaline volcanic rocks is a magmatic association that is not unusual in the WAC. In the Baoulé-Mossi domain, this association has been identified in the Boromo and Houndé belts [12] [13] and interpreted as an evolution of juvenile island arc or oceanic plateau type during the Birimian. This oceanic province is dominated by the basal tholeiitic formation and the magmatic evolution continues to a mature arc, dominated by the calc-alkaline formations. This evolution could be also considered as cause of the petrological diversity of magmatic formations of the Bagoé belt in Syama region.

Acknowledgements

This work is based on unpublished thesis data of Traoré (2017). Resolute Mining is thanked for making before documents and drill cores of the deposit available for study, with special thanks to Pro. Pierre Débat, Dr. Mark Jessell, Dr. Hugues Pobanouh Diarra, Pro. Badié Diourté, and Dr. Mamadou Diawara. Geology department colleagues of FST/USTTB are also thanked for constructive comments and suggestions. We sincerely thank the reviewers and assigned editor of this paper, Mr. Joanna Cheng.

Conflicts of Interest

The authors declare no conflicts of interest regarding the publication of this paper.

References

[1] Rocci, G. (1966) Essai d'interprétation des mesures géochronologiques de la structure de l'Ouest africain. *Science Terre*, **10**, 3-4.

[2] Abouchami, W., Boher, M., Michard, A. and Albarède, F. (1990) A Major 2.1 Ga Event of Mafic Magmatism in West Africa: An Early Stage of Crustal Accretion. *Journal of Geophysical Research*, **95**, 17605-17629. https://doi.org/10.1029/JB095iB11p17605

[3] Boher, M., Abouchami, W., Michard, A., Albarede, F. and Arndt, N.T. (1992) Crustal Growth in West Africa at 2.1 Ga. *Journal of Geophysical Research*: *Space Physics*, **97**, 345-369. https://doi.org/10.1029/91JB01640

[4] Potrel, A., Peucat, J. and Fanning, C. (1998) Archean Crustal Evolution of the West African Craton: Example of the Amsaga Area (Reguibat Rise). U-Pb and Sm-Nd

Evidence for Crustal Growth and Recycling. *Precambrian Research*, **90**, 107-117. https://doi.org/10.1016/S0301-9268(98)00044-8

[5] Lompo, M. (2010) Paleoproterozoic Structural Evolution of the Man-Leo Shield (West Africa). Key Structures for Vertical to Transcurrent Tectonics. *Journal of African Earth Sciences*, **58**, 19-36. https://doi.org/10.1016/j.jafrearsci.2010.01.005

[6] Pouclet, A., Vidal, M., Delor, C., Simeon, Y. and Alric, G. (1996) Le volcanisme birimien du nord-est de la Côte-d'Ivoire, mise en évidence de deux phases volcano-tectoniques distinctes dans l'évolution géodynamique du Paléoprotérozoïque. *Bulletin de la Société géologique de France*, **167**, 529-541.

[7] Pawlig, S., Gueye, M., Klischies, R., Schwarz, S., Wemmer, K. and Siegesmund, S. (2006) Geochemical and Sr-Nd Isotopic Data on Birimian Formations of the Kédougou Kenieba Inlier (Eastern Senegal): Implications on the Paleoproterozoic Evolution of the West African Craton. *South African Journal of Geology*, **109**, 411-442. https://doi.org/10.2113/gssajg.109.3.411

[8] Augustin, J. and Gaboury, D. (2017) Paleoproterozoic Plume-Related Basaltic Rocks in the Mana Gold District in Western Burkina Faso, West Africa: Implications for Exploration and the Source of Gold in Orogenic Deposits. *Journal of African Earth Sciences*, **129**, 17-30. https://doi.org/10.1016/j.jafrearsci.2016.12.007

[9] Dia, A. (1988) Caractères et signification des complexes magmatiques et métamorphiques du secteur de Sandikounda-Laminia (Nord de la boutonnière de Kédougou, Est du Sénégal): Un modèle géodynamique du Birimien de l'Afrique de l'Ouest. Unpublished Ph.D. Thesis, Université de Dakar, Sénégal, 350.

[10] Sylvester, P.J. and Attoh, K. (1992) Lithostratigraphy and Composition of 2.1 Ga Greenstone 197 Belts of the West African Craton and Their Bearing on Crustal Evolution and the Archean-Proterozoic Boundary. *Journal of Geology*, **100**, 377-393. https://doi.org/10.1086/629593

[11] Salah, A., Liégeois, J.P. and Pouclet, A. (1996) Evolution d'un arc insulaire océanique birimien précoce au Liptako nigérien (Sirba): Géochronologie et géochimie. *Journal of African Earth Science*, **22**, 235-254. https://doi.org/10.1016/0899-5362(96)00016-4

[12] Baratoux, L., Metelka, V., Naba, S., Jessell, M.W., Grégoire, M. and Ganne, J. (2011) Juvenile Paleoproterozoic Crust Evolution during the Eburnean Orogeny (~2.2-2.0 Ga), Western Burkina-Faso. *Precambrian Research*, **191**, 18-45. https://doi.org/10.1016/j.precamres.2011.08.010

[13] Béziat, D., Bourges, F., Débat, P., Lompo, M., Martin, F. and Tollon, F. (2000) A Paleoproterozoic Ultramafic-Mafic Assemblage and Associated Volcanic Activity in the West African Craton. *Precambrian Research*, **10**, 25-47. https://doi.org/10.1016/S0301-9268(99)00085-6

[14] Soumaïla, A., Henry, P. and Rossy, M. (2004) Contexte de mise en place des roches basiques de la ceinture de roches vertes birimiennes de Diagorou-Darbani (Liptako, Niger Afrique de l'Ouest); plateau océanique ou environnement d'arc/bassin arrière-arc océanique. *Comptes Rendus de l'Académie des Sciences*, **336**, 1137-1147. https://doi.org/10.1016/j.crte.2004.03.008

[15] Dampare, S.B., Shibata, T., Asiedu, D.K., Osa, S. and Banoeng-Yakubo, B. (2008) Geochemistry of Paleoproterozoic Metavolcanic Rocks from the Southern Ashanti Volcanic Belt Ghana: Petrogenetic and Tectonic Setting Implications. *Precambrian Research*, **162**, 403-423. https://doi.org/10.1016/j.precamres.2007.10.001

[16] De Kock, G.S., Théveniaut, H., Botha, P.M.W. and Gyapong, W. (2012) Timing the Structural Events in the Paleoproterozoic Bolé-Nangodi Belt Terrane and Adjacent

Maluwe Basin, West African Craton, in Central-West Ghana. *Journal of African Earth Sciences*, **65**, 1-24. https://doi.org/10.1016/j.jafrearsci.2011.11.007

[17] Senyah, G.A., Dampare, S.B. and Asiedu, D.K. (2016) Geochemistry and Tectonic Setting of the Paleoproterozoic Metavolcanic Rocks from the Chirano Gold District, Sefwi Belt, Ghana. *Journal of African Earth Sciences*, **122**, 32-46. https://doi.org/10.1016/j.jafrearsci.2015.07.022

[18] Olson, S.F., Diakité, K., Ott, L., Guindo, A., Forb, C.R.B., Winer, N., Hanssen, E., Lay, N., Bradley, R. and Pohl, D. (1992) Proterozoic Syama Gold Deposit, Mali West Africa. *Economic Geology*, **84**, 310-331. https://doi.org/10.2113/gsecongeo.87.2.310

[19] Traoré, D.Y. (2017) Etude métallogénique du district aurifère de Syama (Mali): Analyse comparative de gisements situés sur une même structure lithosphérique éburnéenne. Thèse de doctorat, Université de Toulouse 3 Paul Sabatier, 297.

[20] Gozol, A., Diène, M., Diallo, D.P., Dioh, E., Gueye, M. and N'diaye, P.M. (2015) Petrological and Structural Approach to Understanding the Mechanism of Formation and Development of Paleoproterozoic Calc-Alkaline Volcanic Rocks of West Africa's Craton: An Example of the Mako and Foulde Groups (Kedougou Inlier in Western Senegal). *International Journal of Geoscience*, **6**, 675-691. https://doi.org/10.4236/ijg.2015.67055

[21] Diarra, P.H. (1996) The Geology and Genesis of the Syama Gold Deposit, Mali, West Africa. Thesis Department of Geology, Faculty of Science, University of Southampton, Southampton.

[22] Bassot, J.P. and Dommanget, A. (1986) Mise en evidence d'un accident majeur affectant le protérozoïque inférieur des confins sénégalo-maliens. *Comptes Rendus de l'Académie des Sciences*, **302**, 1101-1106.

[23] Koné, A.Y., Nasr, I.H., Traoré, B., Amiri, A., Inoubli, M.H., Sangaré, S. and Qaysi, S. (2021) Geophysical Contributions to Gold Exploration in Western Mali According to Airborne Electromagnetic Data Interpretations. *Minerals*, **11**, Article No. 126. https://doi.org/10.3390/min11020126

[24] Markwitz, V., Hein, A.A.K., Jessell, M.W. and Millier, J. (2016) Metallogenic Portfolio of the West Africa Craton. *Ore Geology Review*, **78**, 558-563. https://doi.org/10.1016/j.oregeorev.2015.10.024

[25] Sangaré, A., Driouch, Y., Salvi, S., Femenias, O., Féménias, Siebenaller, L., Belkasmi, M., Béziat, D., Dahire, M., Ntarmouchant, A., Adil, S. and Débat, P. (2014) Géologique des minéralisations aurifères du gisement tardi-éburnéen de Kalana (Birimien, Sud-Ouest du Mali). *Bulletin de l'Institut scientifique*, **36**, 85-108.

[26] Traoré, D.Y., Siebenaller, S., Béziat, D. and Bouaré, M.L. (2016) Progressive Gold Mineralization along the Syama Corridor, Southern Mali (West Africa). *Ore Geology Review*, **78**, 586-598. https://doi.org/10.1016/j.oregeorev.2015.11.003

[27] Traoré, D.Y., Bouaré, M.L., Béziat, D., Coulibaly, S. and Koné, A.Y. (2020) Minéralisation de trois gisements aurifère birimiens (Syama, Tabakoroni et Tellem) sur la ceinture de Bagoé au Mali. 11*ieme Symposium Malien sur les Sciences Appliquées* (*MSAS* 2020), Vol. 2, 628-634.

[28] Kushnir, I. (1999) Gold in Mali. *Acta Monanistika*, **4**, 311-318.

[29] Milési, J.P., Feybesse, J.L., Ledru, P., Dommaget, A., Ouédraogo, M.F., Marcoux, E., Prost, A., Vichon, C., Sylvain, J.P., Johan, V., Tegyey, M., Calvex, J.Y., Lagny, P., Abouchami, W., Ankrah, P., Boher, M., Diallo, M., Fabre, M., Henry, C., Lapierre, H., Pons, J., Thiéblemont, D., Touré, S. and Morel, B. (1989) Les minéralisations aurifères de l'Afrique de l'Ouest. *Chronique Recherche Minière*, **497**, 3-98.

[30] Girard, P., Goulet, N. and Malo, M. (1998) Synthèse des données géologiques et

cartographie, 233 Amélioration et Modernisation du centre de documentation, Géologie du Mali. Rapport final, 234, partie II.

[31] Standing, J. (2005) Geological and Structural Mapping in the Syama-Finkolo Prospect Area, Mali, West Africa. Confidential Report by Jigsaw Geoscience Pty Ltd. to Resolute Mining Limited, 29.

[32] Ballo, I., Hein, A.A.K., Guindo, B., Sanogo, L., Ouologuem, Y., Daou, G. and Traoré, A. (2016) The Syama and Tabakoroni Gold Fields, Mali. *Ore Geology Reviews*, **78**, 578-585. https://doi.org/10.1016/j.oregeorev.2015.10.019

[33] Le Bas, M.J. and Streckeisen, A.L. (1991) The IUGS Systematics of Igneous Rocks. *Journal of Geological Society of London*, **148**, 825-833. https://doi.org/10.1144/gsjgs.148.5.0825

[34] Shan, S.J. (1943) The Eruptive Rocks. 2nd Edition, John Wiley, New York, 444 p.

[35] Le Bas, M.J., Lemaître, R.W., Streckeisen, A. and Zanettin, B. (1986) Une classification chimique des roches volcaniques basée sur le diargramme de silice alcaline totale. *Journal de Pétrologie*, **27**, 745-750. https://doi.org/10.1093/petrology/27.3.745

[36] Cann, J.R. (1970) Rb, Sr, Y, Zr and Nb in Some Ocean Floor Basaltic Rocks. *Earth and Planetary Science Letters*, **10**, 7-11. https://doi.org/10.1016/0012-821X(70)90058-0

[37] Condie, K.C. (2005) High Field Strength Element Ratios in Archean Basalts: A Window to Evolving Sources of Mantle Plumes? *Lithos*, **79**, 491-504. https://doi.org/10.1016/j.lithos.2004.09.014

[38] Manya, S., Makenya, A., Maboko, H. and Nakamura, E. (2007) The Geochemistry of High-Mg Andesite and Associated Adakitic Rocks in the Usoma-Mara Greenstone Belt, Northern Tanzania: Possible Evidence for Neoarchean Ridge Subduction? *Precambrian Research*, **159**, 241-259. https://doi.org/10.1016/j.precamres.2007.07.002

[39] Miyashiro, A. (1978) Nature of Alkaline Volcanic Rock Series. *Contributions to Mineralogy and Petrology*, **66**, 91-104. https://doi.org/10.1007/BF00376089

[40] McDonough, W.F. and Sun, S.S. (1995) The Composition of the Earth. *Chemical Geology*, **120**, 223-253. https://doi.org/10.1016/0009-2541(94)00140-4

[41] Sun, S.S. and McDonough, W.F. (1989) Chemical and Isotopic Systematics of Oceanic Basalts: Implications for Mantle Composition and Processes. In: Saunders, A.D. and Norry, M.J., Eds., *Magmatism in the Ocean Basins*, Geological Society, Special Publication No. 42, London, 313-345. https://doi.org/10.1144/GSL.SP.1989.042.01.19

[42] Weaver, B.L. and Tarney, J. (1981) The Scourie Dyke Suite: Petrogenesis and Geochemical Nature of the Proterozoic Sub-Continental Mantle. *Contributions to Mineralogy and Petrology*, **78**, 175-188. https://doi.org/10.1007/BF00373779

[43] Barrett, T.J. and MacLean, W.H. (1997) Volcanic Sequences, Litho-Geochemistry and Hydrothermal Alteration in Some Bimodal VMS Systems. In: Barrie, C.T. and Hannington, M.D., Eds., *Volcanics-Associated Massive Sulfide Deposits: Processes and Examples in Modern and Ancient Settings*, GeoScienceWorld, Alexandria, 105-133.

[44] Rock, N.M.S. (1987) The Nature and Origin of Lamprophyres: An Overview. In Fitton, J.G. and Upton, B.G.J., Eds., *Alkaline Igneous Rocks*, Geological Society Special Publications No. 30, London, 191-226. https://doi.org/10.1144/GSL.SP.1987.030.01.09

[45] Béziat, D., Bourges, F., Ddébat, P., Lompo, M., Tollon, F. and Zonou, S. (1998) Albitites et listvénites: Sites de concentration aurifère inédits dans les ceintures de roches

vertes birimiennes fortement hydrothermalisées du Burkina Faso. *Bulletin de la Société géologique de France*, **169**, 563-571.

[46] Karsli, O., Dokuz, A., Kaliwoda, M., Uysal, I., Aydin, F., Kandemir, R. and Fehr, K.T. (2014) Geochemical Fingerprints of Late Triassic Calc-Alkaline Lamprophyres from the Eastern Pontides, NE Turkey: A Key to Understanding Lamprophyre Formation in a Subduction-Related Environment. *Lithos*, **196**, 181-197. https://doi.org/10.1016/j.lithos.2014.02.022

[47] Orozco-Garza, A., Dostal, J., Keppie, J.D. and Paz-Moreno, F.A. (2013) Mid-Tertiary (25-21 Ma) Lamprophyres in NW Mexico Derived from Subduction-Modified Subcontinental Lithospheric Mantle in an Extensional Back Arc Environment Following Steepening of the Benioff Zone. *Tectonophysics*, **590**, 59-71. https://doi.org/10.1016/j.tecto.2013.01.013

[48] Chen, Y., Yao, S. and Pan, Y. (2014) Geochemistry of Lamprophyres at the Daping Gold Deposit, Yunnan Province China: Constraints on the Timing of Gold Mineralization and Evidence for Mantle Convection in the Eastern Tibetan Plateau. *Journal of Asian Earth Sciences*, **93**, 129-145. https://doi.org/10.1016/j.jseaes.2014.07.033

[49] Ross, P.S. and Bédard, J.H. (2009) Magmatic Affinity of Modem and Ancient Sub Alkaline Volcanic Rocks Determined from Trace Element Discriminant Diagrams. *Canadian Journal of Earth Sciences*, **464**, 823-839. https://doi.org/10.1139/E09-054

[50] Polat, A. and Kerrich, R. (2002) Nd-Isotope Systematics of ~2.7 Ga Adakites, Magnesian Andesites, and Arc Basalts, Superior Province: Evidence for Shallow Crustal Recycling at Archean Subduction Zones. *Earth and Planetary Science Letters*, **202**, 345-360. https://doi.org/10.1016/S0012-821X(02)00806-3

[51] Hollings, P. and Kerrich, R. (2004) Geochemical Systematics of Tholeiites from 2.86 Ga Pickle Crow Assemblage, Northwestern Ontario: Arc Basalts with Positive and Negative Nb-Hf Anomalies. *Precambrian Research*, **134**, 1-20. https://doi.org/10.1016/j.precamres.2004.05.009

[52] Pearce, J.A. and Peate, D.W. (1995) Tectonic Implications of the Composition of Volcanic Arc Magmas. *Earth and Planetary Sciences*, **23**, 251-285. https://doi.org/10.1146/annurev.ea.23.050195.001343

[53] Manikyamba, C., Kerrich, R., Naqvi, S.M. and Ram Mohan, M. (2004) Geochemical Systematics of Tholeiitic Basalt from the 2.7 Ga Ramagiri-Hungund Composite Greenstone Belt, Dharwar Craton. *Precambrian Research*, **134**, 21-39. https://doi.org/10.1016/j.precamres.2004.05.010

[54] Kerr, A.C. and Mahoney, J.J. (2007) Oceanic Plateaus: Problematic Plumes, Potential Paradigms. *Chemical Geology*, **241**, 332-353. https://doi.org/10.1016/j.chemgeo.2007.01.019

[55] Velásquez, G. (2012) First Occurrence of Paleoproterozoic Oceanic Plateau in the Guinea Shield: The Gold-Bearing El Callao Formation, Venezuela. Thèse Doct, Université Paul Sabatier, Toulouse.

[56] Sangaré, A. (2008) Les roches ultramafiques et mafiques paléoprotérozoïques de la ceinture de roches vertes de Kadiolo (Mali). Pétrologie, évolution et ressources minérales associées. Master Géosciences et Ressources Minérales. Université Sidi Mohamed Ben Abdellah, 60 p.

[57] Dioh, E., Béziat, D., Débat, P., Grégoire, M. and Ngom, M. (2006) Diversity of the Paleoproterozoic Granitoids of the Kédougou Inlier (Eastern Senegal): Petrographical and Geochemical Constraints. *Journal of African Earth Science*, **44**, 351-371. https://doi.org/10.1016/j.jafrearsci.2005.11.024

[58] Lahondère, D., Thiéblemont, D., Tegyey, M., Guerrot, C. and Diabaté, B. (2002)

First Evidence of Early Birimian (2.21 Ga) Volcanic Activity in Upper Guinea: The Volcanics and Associated Rocks of the Niani Suite. *Journal of African Earth Sciences*, **35**, 417-431. https://doi.org/10.1016/S0899-5362(02)00145-8

[59] McNeil, A.M. and Kerrich, R. (1986) Archean Lamprophyre Dikes and Gold Mineralization, Ontario. The Conjunction of LILE-Enriched Magmas, Deep Crustal Structures and Gold Concentrations. *Journal of Earth Science*, **23**, 324-343. https://doi.org/10.1139/e86-035

[60] Barley, M.E., Eisenlohr, B.N., Groves, D.I., Perring, C.S. and Vearncombe, J.R. (1989) Late Archean Convergent Margin Tectonics and Gold Mineralization: A New Look at the Norseman Wiluna Belt. *Western Australia Geology*, **17**, 826-829. https://doi.org/10.1130/0091-7613(1989)017<0826:LACMTA>2.3.CO;2